Weak lensing of the high redshift SNIa sample

Liliya L.R. Williams^{1*} and Jeeseon Song^{1*}†

¹ Astronomy Department, University of Minnesota, Minneapolis, MN 55455, USA

26 July 2021

ABSTRACT

The current sample of high-redshift Supernova Type Ia, which combines results from two teams, High-z Supernova Search Team and Supernova Cosmology Project, is analyzed for the effects of weak lensing. After correcting SNe magnitudes for cosmological distances, assuming recently published, homogeneous distance and error estimates, we find that brighter SNe are preferentially found behind regions (5-15 arcmin radius) which are overdense in foreground, $z \sim 0.1$ galaxies. This is consistent with the interpretation that SNe fluxes are magnified by foreground galaxy excess, and demagnified by foreground galaxy deficit, compared to a smooth Universe case. The difference between most magnified and most demagnified SNe is about 0.3-0.4 mag. The effect is significant at > 99% level. Simple modeling reveals that the slope of the relation between SN magnitude and foreground galaxy density depends on the amount and distribution of matter along the line of sight to the sources, but does not depend on the specifics of the galaxy biasing scheme.

Key words: gravitational lensing – supernovae: general

INTRODUCTION

The effects of weak gravitational lensing by the large-scale structure have been detected in several samples of high redshift QSOs, intermediate redshift galaxies, and BATSE GRBs. In the case of point sources, QSOs and GRBs, weak lensing manifests itself as angular (anti-)correlations between these sources and foreground inhomogeneously distributed mass (Williams & Frey 2003; Benitez et al. 2001; Williams & Irwin 1998; Benitez & Martinez-Gonzalez 1997), while in the case of galaxies weak lensing is detected through its coherent shear effect (see Refregier (2003) for a recent review). In principle, there is another, more direct way of detecting weak lensing, which uses fluxes of standard candles. If the observed magnitudes of standard candles are corrected for cosmological distances then the effect of lensing can be seen: brighter sources will lie behind regions of mass density excess, while fainter ones will have mass deficits in their foregrounds.

The best example of cosmological standard candle, Supernovae Type Ia (SNIa) have been extensively observed with the purpose of determining the global geometry of the Universe (Tonry et al. 2003; Perlmutter et al. 1999; Garnavich et al. 1998; Riess et al. 1998). Nuisance effects like evolution, variations in individual SN, and gray dust

extinction have been studied theoretically and observationally, and have either been corrected for or shown to be

small. Weak lensing, another nuisance effect has been ad-

dressed theoretically by several authors (Amanullah et al.

2003; Metcalf 1999; Holz 1998; Wambsganss et al. 1997)

and found to be unimportant given the current uncertain-

ties. For example, Wambsganss et al. (1997) used ray trac-

ing through cosmological simulations and found that the

lensing induced dispersions on truly standard candles are

0.04 and 0.02 mag at redshift z = 1 and z = 0.5, respec-

tively, in a COBE-normalized cold dark matter universe with

 $\Omega_m = 0.4, \ \Omega_{\Lambda} = 0.6, \ H_0 = 65 \text{km/s/Mpc} \ \text{and} \ \sigma_8 = 0.79.$

These are small variations compared to the current errors

which are $\gtrsim 0.2$ mag. Even though weak lensing effects are

estimated to be small for $z_s < 1$, they are predicted to be

non-negligible for higher redshift sources, so it is not surpris-

ing that the highest redshift SNIa, SN1997ff at $z_s = 1.755$

has been examined by several authors (Benitez et al. 2002;

Moertsell et al. 2001; Lewis & Ibata 2001) for the effects of

weak lensing due to galaxies along the line of sight.

Present day high-z SNIa samples are dominated by lower redshift SNe, and so have not been examined for the effects of lensing. The main goal of this work is to determine if the observed fluxes of the cosmologically distant SNIa have suffered significantly from lensing induced (de-) amplifications.

^{*} E-mail: llrw@astro.umn.edu (LLRW); jsong4@astro.uiuc.edu (JS)

[†] Present address: Department of Astronomy 133 Astronomy Building, 1002 W. Green St. Urbana, IL 61801, USA

2 DATA

The largest homogeneous compilation of SNIa has been recently published by Tonry et al. (2003): Table 15 of that paper contains 74 SNe at $z_s \geqslant 0.35$. The authors use four different light curve fitting methods (MLCS, $\Delta m_{15}(B)$, modified dm15, and Bayesian Adapted Template Match) to estimate distances to SNe. The final quoted distance is the median of the estimates of the four individual methods, and the uncertainty is the median of the error of the contributing methods. The analysis presented in Tonry et al. (2003) yields values of the global cosmological parameters; if a flat model is assumed, then $\Omega_m=0.28$ and $\Omega_{\Lambda}=0.72$. We use these values in all the analysis of the present paper.

As tracers of foreground mass density we use APM galaxies (Irwin et al. 1994). APM provides near full coverage of the sky in the Northern and Southern Hemispheres, at $|b| \gtrsim 20^{\circ}$. In our analysis we use only the central $r=2.7^{\circ}$ of APM plates. Since the plate centres are separated by $\sim 5^{\circ}$, there exist small portions of the sky that are not covered by any plate. As a result of these cuts, only 55 of the 74 SNe lie on the usable parts of APM plates.

The median redshift of the 55 SNe is 0.47. Since most of the SNe have rather low redshifts, care must be taken to ensure that galaxies are foreground to the SNe. Furthermore, because SNe span a large range of nearby redshifts, from $z_s = 0.35$ to 1.2, the optimal lens redshift z_l will depend on z_s much more compared to a typical case where sources (say, QSOs) are at $z_s \sim 1-3$ and so the redshift of optimal lenses is roughly independent of z_s . In our analysis we adjust z_l for each SN source by selecting the appropriate limiting apparent magnitude, mag gal lim for APM galaxies on red plates. Maddox et al. (1996) gives an empirical expression for the median redshift z_{med} of a galaxy sample with a given faint magnitude flux cutoff. This median redshift can be equated with the optimal lens redshift z_l , and hence the magnitude limit of the foreground galaxies can be determined for every SN separately. However, there is a small catch. For $z_s = 0.4$ optimal $z_l = 0.174$. The galaxy redshift distribution whose median redshift $z_{med} = 0.174$ has a considerable tail extending beyond z = 0.4. To avoid the problem of source/lens redshift overlap we use $z_{med} = z_l/2$, where factor of 2 was chosen arbitrarily. We explore the dependence of the results on this factor in Section 4.

3 ANALYSIS

Around every SN we draw a circle of radius $\theta=10'$, and count the number of galaxies, $n_{gal,D}$, in the appropriate magnitude range. This number is compared to the average number density in control circles, $\langle n_{gal,R} \rangle$. Fractional galaxy excess is $\delta n_{gal} = n_{gal,D}/\langle n_{gal,R} \rangle -1$. Control circles are confined to the same APM plate as the SN, and to the same distance from the plate centre as the SN (to reduce the effects of vignetting); however, scattering the control circles randomly on the plate does not change the results significantly. For each SN we also calculate $N_{>}/N$, where $N_{>}$ is the number of control circles, out of total N, that have less

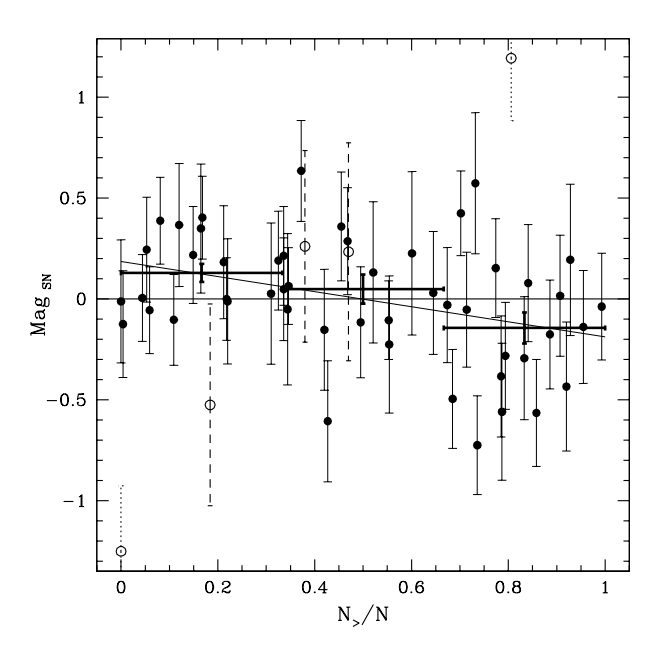


Figure 1. Absolute magnitudes of SNIa (modulo a constant off-set) versus the foreground galaxy density. Magnitudes were obtained assuming $\Omega_m = 0.28$, and $\Omega_{\Lambda} = 0.72$, and extinction, K-corrected distances from Tonry et al. (2003). $N_>/N$ is a measure of the number density of foreground galaxies in circles of radius $\theta = 10'$ around SNe (see Section 3 for details). There are a total of 55 sources (with magnitude errors), but only 50 (filled points) are used in the analysis. The 50 points are grouped into three bins, whose horizontal size is shown as thick horizontal "error-bars". The corresponding vertical error-bars show the deviation of the mean of the points in each bin (the rms is 4 times larger), and the intersection of the thick lines are the averages of the Mag_{SN} of SNe in each bin. The thin slanting line is the best-fit to 50 SNe, and has a slope $\beta = -0.373$. The significance of the correlation is > 99%.

galaxies in them than the circle around the SN. In other words, $N_>/N$ is the rank of the SN circle among its control 'peers'. If SNe are randomly distributed with respect to the foreground galaxies, then average $\langle N_>/N\rangle = 0.5$. If SNe have an excess (deficit) of galaxies in front of them then their $\langle N_>/N\rangle$ will be greater (less) than 0.5. Analogous to the medians being more stable than averages, $N_>/N$ rank statistic is more stable than δn_{gal} .

Figure 1 shows absolute magnitudes, M_{SN} , and $N_{>}/N$ ranks of 55 SNe found on APM plates. The effect of flux dimming due to cosmological distances has been taken out, i.e. all the SNe have been 'brought' to the same redshift; the constant magnitude offset on the vertical axis is irrelevant for this work. There are two SNe whose magnitudes make them $> 3\sigma$ outliers, SN1997O, and SN1997bd represented by empty circles with dotted line error-bars. We exclude these from our analysis.²

² Of our 55 SNe, SN1997bd has the highest host-galaxy extinction, $\langle A_v \rangle$ as quoted in Tonry et al. (2003). SN1997O and SN1994H were excluded from the primary fit (Fit C) by the analysis of Perlmutter et al. (1999). We do not exclude SN1994H from our analysis, but if we did it would improve the trend, as its coordinates on Fig. 1 are (0.427; -0.606).

 $^{^1\,}$ SN1997ff at $z_s=1.755$ is not in our sample: it fell in the cracks between the APM plates.

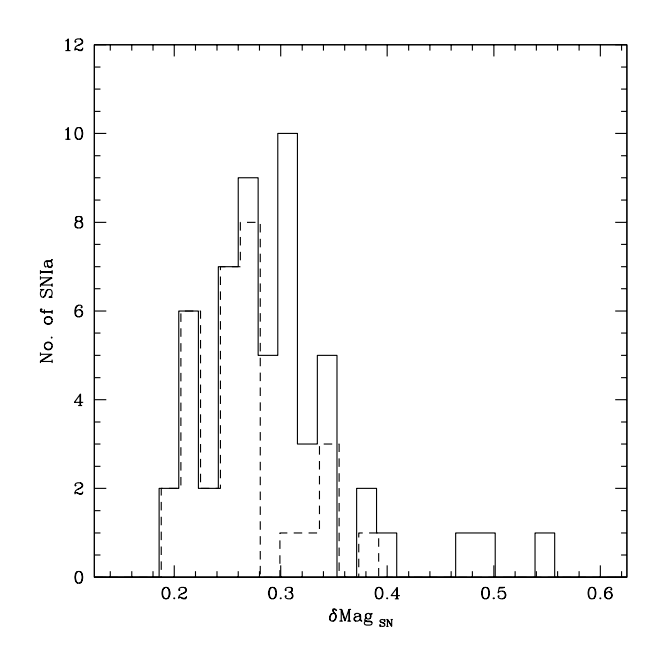


Figure 2. Histogram of SNIa magnitude errors, $\delta M_{SN} = 5 \ \delta \log(d)$. Distance errors, $\delta \log(d)$ were derived by Tonry et al. (2003), and listed in column 9 of their Table 15. The solid histogram is for 55 SN; the dashed line represents 31 SN from the High-z Supernova Search Team. The 3 outlier SNe with $\delta M_{SN} > 0.45$ are not used in the present analysis.

The distance (or, magnitude) errors, as estimated by Tonry et al. (2003) for the 55 SNe are shown in Fig. 2, as the solid line histogram. The dashed line represents the subsample of 31 SNe from High-z Supernova Search Team (Tonry et al. 2003), whose errors appear to be generally smaller than those of the Supernova Cosmology Project (Perlmutter et al. 1999). We use SNe from both the groups, but exclude three outliers in Fig. 2, whose $\delta M_{SN} > 0.45$. In Fig. 1 these are represented by empty circles with dashed line error-bars. Thus, we exclude a total of 5 SNe from our analysis, leaving us with 50, shown as the solid points in Fig. 1.

These 50 SNe exhibit a relation between their M_{SN} and $N_>/N$, in the sense that brighter SNe have an excess of galaxies in their foregrounds. For illustration purpose only, we bin the 50 SNe into three bins; Fig. 1 shows the extent of the bins and the deviation of the mean of the SNe magnitudes in each bin as thick lines.

The best-fit line to the 50 SNe in Fig. 1 has a slope $\beta=-0.373$, and is shown as a thin slanting line. This fit does not include magnitude errors. To include the errors we do the following. We calculate the best-fit slope for 10,000 realizations of the data, where each data point's SN magnitude is replaced by a randomly picked magnitude from a Gaussian distribution centred on the actual magnitude value, and having width equal to the quoted error. This procedure correctly incorporates the information contained in the errors, and produces a distribution of best-fit slopes, which is shown as a solid line histogram in Fig. 3. This distribution shows that the median best-fit slope is $\beta=-0.372$, while $\beta=0$ (i.e. a case of no correlation) is ruled out at 99.80% confidence level. Had we used 53 SNe (i.e. had we not exluded

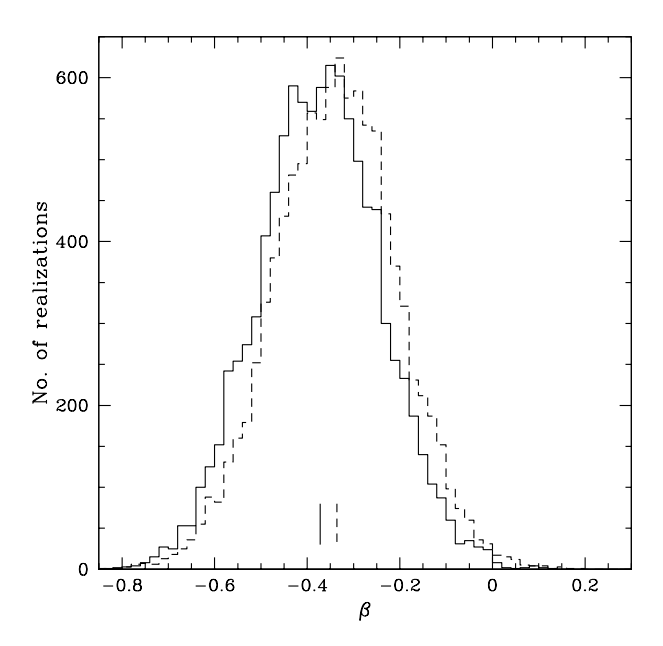


Figure 3. How do the SN distance errors affect the best-fit slope, β ? The histograms show the distribution of derived β values in 10,000 realizations of the data. The solid (dashed) line histogram represents results using 50 (53) SNe. The short vertical lines at the bottom of the plot indicate the medians of the distributions.

the 3 SNe with large distance errors), the median best-fit slope would gave been $\beta=-0.336$, while $\beta=0$ would have been ruled out at 99.37% confidence level. The corresponding distribution of β slopes is shown as the dashed line in Fig. 3.

Next, we determine the likelihood of this relation arising by chance. To that end, we estimate the significance of the relation in two ways. First, we assign random positions to SNe (keeping these control SNe on the same APM plate as the original source), and redo all the analysis. We repeat this 1000 times, and in 8 cases we find $\beta \leq -0.373$, implying statistical significance of 99.2%. Second, we take the list of observed M_{SN} values and randomly reassign them to observed SN sky positions. 10,000 randomized SNe samples are created in this fashion, and only 0.5% of these have $\beta \leq -0.373$. Based on these two tests we conclude that the significance of the $M_{SN}-N_{>}/N$ relation is better than 99%.

These results are consistent with weak gravitational lensing, which would amplify SNe found behind more nearby mass concentrations, as traced by APM galaxies. Alternatively, the results could be due to the action of Galactic dust, which will obscure certain directions of the sky making galaxies less numerous and SNe fainter. We consider Galactic dust further in Section 7; in Sections 5 and 6 we proceed on the assumption that weak lensing is responsible to the $M_{SN}-N_{>}/N$ relation.

4 FURTHER TESTS

The distribution of SNe points in Fig. 1 depends on specific choices that we made for certain parameters, in particular we chose circles of radius $\theta=10'$ and galaxy magnitude

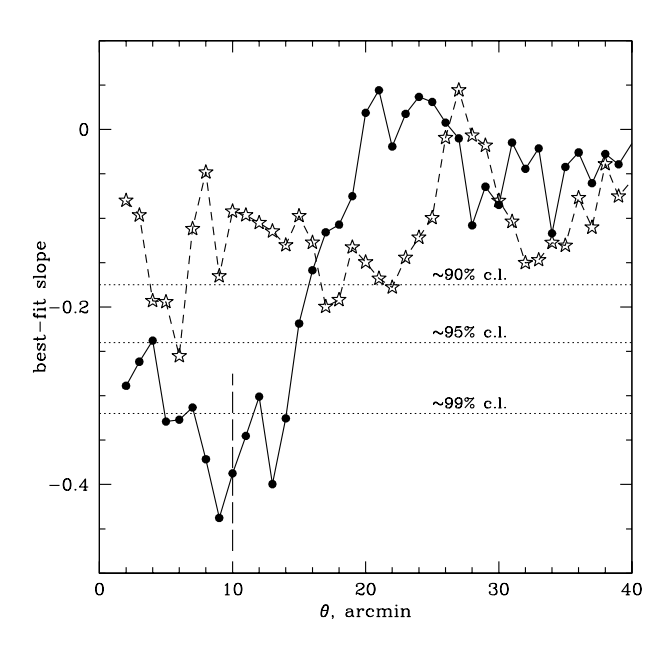


Figure 4. Control tests: varying the aperture radius, θ of circles around SNe. The vertical axis shows β , the slope of the best-fit line to the relation of the type shown in Fig 1. The filled circles represent cases where galaxies were counted around SN; stars symbols represent cases where Galactic stars were used instead (i.e. control experiment). The dotted lines denote, approximately, the levels of statistical confidence. The dashed vertical line indicates radius θ used in the analysis of Section 3.

limit such that $z_{med} = z_l/x$, where x = 2 (see Section 2). How would the results change if different choices were made? In other words, how robust is our result, would it disappear had we picked a different set of parameters?

Figure 4 shows the effect of changing θ . The vertical axis is β , the best-fit to the $M_{SN}-N_{>}/N$ relation in each case. Filled points represent cases where galaxies were counted and used to determine the $N_>/N$ rank, while star symbols represent cases where Galactic stars were used instead. As expected, δn_{stars} do not correlate with SNe magnitudes, and the values of the best-fit slopes are near zero. However, because the APM star-galaxy classifier is not perfect, some 'stars' are actually galaxies, which accounts for some signal being seen when using δn_{stars} . Horizontal dotted lines mark the approximate location of 90%, 95%, and 99% confidence levels. These are only approximate because every point in the plot will have its own significance level, but because the number of SNe contributing to each point is the same in each case, and the total dispersion in SNe magnitudes is the same, same β values have about the same significance, regardless of θ . We note that for very small θ the galaxy numbers become very small, and Poisson noise drowns out any $M_{SN}-N_{>}/N$ correlation that might exist, so the upturn in the values of the best-fit slope at small θ is probably not real. The dashed vertical line marks the θ value used in Section 3. We conclude that significant $M_{SN}-N_{>}/N$ anti-correlations occur only with galaxies and not with Galactic stars (which serve as a control sample), and only for $5' \lesssim \theta \lesssim 15'$.

Figure 5 shows the effect of changing the median redshift, $z_{med} = z_l/x$ of the APM galaxies, or equivalently,

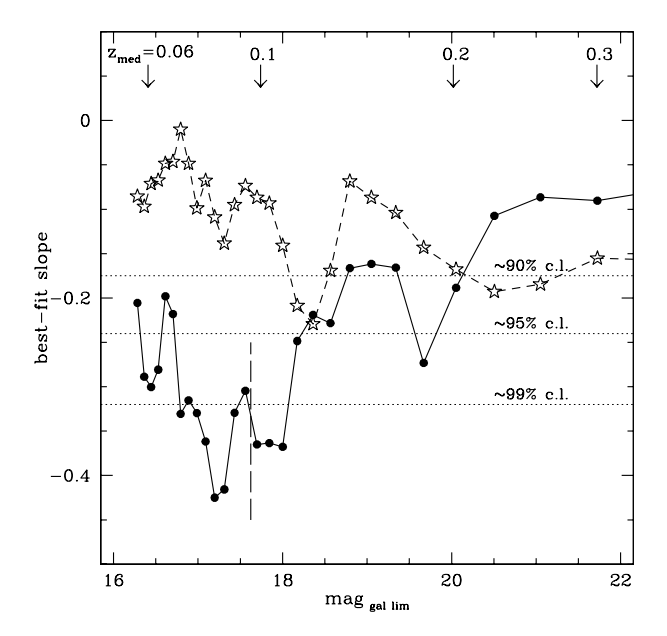


Figure 5. Control tests: varying the apparent magnitude limit of galaxies and the corresponding median redshift z_{med} . Similar to Fig. 4; see Section 4 for details.

mag gal lim. The hidden variable which is varied along the horizontal axis is x. Since each SN has a different value of z_l and hence mag $g_{al\ lim}$, depending on its z_s , there is no unique way of labeling the horizontal axis by using galaxy magnitudes, or redshifts. We label that axis by assuming $z_s = 0.47$, the median of the SNe redshift distribution. At the top of the plot we show how galaxy magnitude limit on the horizontal axis translates into the median galaxy redshift (for a specific case of $z_s = 0.47$). We see that significant anticorrelation between M_{SN} and $N_{>}/N$ of foreground galaxies occurs for galaxies with $z_{med} \lesssim 0.12$. Using Galactic stars instead of galaxies produces no significant results. The value we used in Section 3 is shown with a vertical dashed line, and corresponds to $z_{med} \approx 0.1$. As in Fig. 4 the upturn in the best-fit slope values at bright mag gal lim is probably due to Poisson noise. The range of redshifts of APM galaxies that act as the best lenses for SNe are $\sim 0.05 - 0.2$; more distant galaxies show no signal, as expected, if lensing is the correct interpretation of the data, because more distant galaxies are either too close to SNe in redshift or are actually at the same

A number of other tests have been carried out as well. For example, instead of using a z_s -dependent mag $g_{al\ lim}$, we tried fixed values of 17.5, 18.0, 18.5, which gave, $\beta = -0.35, -0.31, -0.27$, respectively, comparable to, but somewhat smaller than those seen in Fig. 5. This is not surprising: z_s -dependent galaxy magnitude limits pick optimal lens redshifts for each source, thus maximizing the observed lensing signature.

We also reran the analysis with subsamples of the entire 50-source sample. We split the SNe according to the teams: 20 Supernova Cosmology Project SNIa gave a $M_{SN}-N_{>}/N$ anti-correlation significant at 95.8%, while the corresponding significance level for the 30 SNe from the High-z Supernova Search Team is 96%. Because the quality of UKST

APM (Southern Hemisphere) plates is higher than POSS APM (Northern Hemisphere) plates, and because there is some overlap between plates along the equator, we used UKST plates whenever possible. Redoing the analysis using only the 36 UKST SNe we get the best fit slope $\beta=-0.46$ at a significance level of 99.6%, while the 14 POSS SNe had $\beta=-0.11$ and the correlation was not significant, which is not surprising given the size of this subsample. Splitting the whole sample into low and high redshift groups we get the following results: 25 SNe with $z_s < 0.47$ have a slope $\beta=-0.37$ at 96.8%, while 25 SNe with with $z_s \geqslant 0.47$ have a slope $\beta=-0.23$ at 88.9%. These tests suggest that the $M_{SN}-N_>/N$ relation has a physical origin (weak lensing or Galactic dust), and is not an artifact arising form one subset of the data.

5 MODELING THE OBSERVATIONS

In this Section we adopt the weak lensing interpretation of the $M_{SN}-N_{>}/N$ relation. Our simple lensing model does not use the individual values of z_s , and the optimal redshift distribution of the corresponding lenses. In lieu of these parameters we use the lensing optical depth of the matter traced by the galaxies, κ_0 . For a fixed global geometry, κ_0 depends on z_s and the redshift distribution of the mass traced by the galaxies. We assume that the APM galaxies faithfully trace the mass up to some redshift, z_t , then

$$\kappa_0 = \Omega_m \ \rho_{crit} \ (c/H_0)$$

$$\times \int_0^{z_t} \frac{(1+z)^2}{[\Omega_m (1+z)^3 + \Omega_{\Lambda}]^{1/2} \ \Sigma_{crit}(z, z_s)} \ dz, \quad (1)$$

In that case, projected fractional mass excess is $\delta n_{mass} = \kappa/\kappa_0$, where κ is the convergence, with respect to a smooth Universe (filled beam) for the corresponding line of sight. In the weak lensing regime source amplification $A \approx (1 + 2\kappa)$; A = 1 for an unlensed source. The smallest value that κ can attain is minus the total optical depth, $-\kappa_0$, which corresponds to emptying out all the mass along the line of sight from the observer to z_t .

In addition to the value for κ_0 , our model has three ingredients, (1) mass distribution, i.e. a probability distribution (pdf) for δn_{mass} , which is related to κ pdf, (2) a biasing scheme, which relates δn_{mass} to the projected fractional galaxy number density excess, δn_{gal} , and (3) the dispersion in the intrinsic magnitudes of SNIa's. Given this information we generate synthetic SNIa samples, with 50 sources each, then compute $N_{>}/N$ each SN, and the observed SN magnitude, M_{SN} . The slope of the best-fit line to the $M_{SN}-N_{>}/N$ relation, β is then used to test how well a given model reproduces the observations.

Because our model assumes the same z_l distribution for all sources, the value of β to compare our models' predictions to should be the one obtained by using a constant mag $g_{al\ lim} \approx 18$, i.e. $\beta \approx -0.3$ (see fourth paragraph in Section 4).

The specifics of the three model ingredients, and the associated model parameters are described later in this Section. The goal of the modeling is to determine what set of parameters can reproduce the observations, i.e. have $\beta \leq -0.3$. We are particularly interested in what effect biasing has on the results. It is often suggested that the large amplitude of

QSO-galaxy correlations mentioned in the Introduction is, at least in part, due to the fact that biasing is not a simple linear, one-to-one mapping from δn_{mass} to δn_{gal} . QSO-galaxy correlation function (ω_{QG}), galaxy autocorrelation (ω_{GG}) and the matter fluctuation power spectrum (P_k) are related by

$$\omega_{QG} \propto b^{-1} \omega_{GG} \propto b P_k,$$
 (2)

where b is the biasing parameter. This means that ω_{QG} probes a *combination* of b and P_k . Thus, for a given P_k , ω_{QG} can be enhanced with positive biasing, especially if it is non-linear on relevant spatial scales.

The important difference between weak lensing induced QSO-galaxy correlations and the effect on standard candles we have studied here is that in the latter case biasing plays a minor role. The slope of the $M_{SN}-N_{>}/N$ relation is most sensitive to the mass distribution. Our modeling demonstrates this later; first, we described the specifics of the three model ingredients.

5.1 Mass distribution

5.1.1 The standard mass distribution

Based on the results from cosmological N-body simulations (Jain et al. 2000) the shape of the probability distribution function (pdf) of κ is very roughly Gaussian, but asymmetric, with the most probable κ , which we call κ_m being less than 0, i.e. most sources are deamplified. The tail of the κ distribution extends to high positive values of κ . We use these published results of Jain et al. (2000) to construct an approximate shape for our κ pdf:

$$p(\kappa) = \begin{cases} exp\left(-\left[\kappa - \kappa_m\right]^2 / 2\sigma_{\kappa_1}\right), & \text{for } \kappa > \kappa_m \\ exp\left(-\left[\kappa - \kappa_m\right]^2 / 2\sigma_{\kappa_2}\right), & \text{for } \kappa \leqslant \kappa_m \end{cases}$$
(3)

The pdf is a combination of two half-Gaussians, with two widths, σ_{κ_1} and σ_{κ_2} , which describe the high κ and the low κ sides of the pdf respectively. The location of the peak of the pdf, κ_m is adjusted such that the average κ is 0, which implies

$$\kappa_m = \sqrt{2/\pi} \, (\sigma_{\kappa_2} - \sigma_{\kappa_1}). \tag{4}$$

 κ_m is always negative, since the skewness of the pdf dictates that $\sigma_{\kappa_1} > \sigma_{\kappa_2}$. From the numerically computed pdfs of Jain et al. (2000) we estimate that for a flat $\Omega_m = 0.3$ model, where the sources are at $z_s \approx 0.5-1$, and the smoothing scale is $\sim 5'-10'$, the following approximations apply: $\sigma_{\kappa_1}/\sigma_{\kappa_2} \approx 2.6$, and $\sigma_{\kappa_1} \approx \kappa_0/3.6$. Thus we now have a realistic κ pdf, appropriate for a standard cosmology with standard mass distribution. Figure 7(d) shows such a pdf as a short-dash line.

5.1.2 Non-standard mass distribution: bifocal lens

In addition to the standard κ pdf described above, we also try an extreme form for κ pdf obtained using the "bifocal lens" mass distribution proposed by Kovner (1991):

$$p(A) = \frac{1 - A_2}{A_1 - A_2} \delta(A - A_1) + \frac{A_1 - 1}{A_1 - A_2} \delta(A - A_2)$$
 (5)

where δ is the Kronicker's delta function, $A_1 > 1$, and $A_2 < 1$. For a fixed κ_0 , this pdf can produce more pronounced

6

lensing effects than the standard pdf, if A_2 is assigned the smallest allowable value, and A_1 is made very large. This is because the standard pdf has a large probability near A=1, while the bifocal pdf avoids such values altogether.

The distribution of mass corresponding to eq. 5 is unrealistic. One can make it somewhat realistic by allowing a range of A_1 and A_2 values. We do the following: for any one line of sight we randomly pick A_1 and A_2 from specified ranges, using flat priors, and eq. 5 sets the probability distribution of the two amplifications. We use two sets of ranges: (1) $1 < A_1 \le (1+5 \kappa_0)$ and $(1-\kappa_0) < A_2 \le 1$ (we will call this model bifocal I model), (2) $1 < A_1 \le (1 + 10 \kappa_0)$ and $(1-2 \kappa_0) < A_2 \leqslant 1$ (we will call this bifocal II). The corresponding κ pdfs, obtained by considering many lines of sight are shown in Fig. 7(d) as a solid line for bifocal II and as a long-dash line for bifocal I. In bifocal II the minimum value of A_2 is the minimum allowed value; the other limits on A's were picked arbitrarily. For comparison, the standard κ pdf of Section 5.1.1 is also shown, as the short-dash line. Optical depth of $\kappa_0 = 0.02$ was assumed for all three. Compared to a standard pdf, bifocal pdfs imply that most of the lines of sight are rather empty, and there are a few lines of sight with very high values of κ .

5.2 Biasing scheme

Projected fractional mass excess, δn_{mass} is related to the observationally accessible quantity, δn_{gal} through biasing. We chose "power law" biasing, motivated by numerical simulations of Cen & Ostriker (1993) and Dekel & Lahav (1999),

$$(1 + \delta n_{gal}) = \begin{cases} (1 + \delta n_{mass})^{\alpha_1} + b_s (1 + \delta n_{mass}), & \text{for } \delta n_{mass} > 0\\ (1 + \delta n_{mass})^{\alpha_2} + b_s (1 + \delta n_{mass}), & \text{for } \delta n_{mass} \leqslant 0 \end{cases}$$
(6)

where the power law part allows the biasing to be non-linear, with different indexes depending on the sign of δn_{mass} , while b_s is a stochastic biasing component which is chosen randomly for each SN; b_s distribution has a Gaussian shape and width σ_{b_s} . Factor $(1 + \delta n_{mass})$ multiplying b_s ensures that the dispersion in δn_{gal} is reduced in underdense regions. Qualitatively, the δn_{gal} vs. δn_{mass} relations produced by eq. 6 look similar to those in Fig.1 of Dekel & Lahav (1999).

5.3 Dispersion in the intrinsic SNIa magnitudes

We assume that the dispersion in magnitude about the perfect standard candle case has a Gaussian shape, with width σ_{SN} .

6 RESULTS OF MONTE CARLO SIMULATIONS

Each model has five independent parameters:

 $\{\kappa_0, \alpha_1, \alpha_2, \sigma_{b_s}, \sigma_{SN}\}$. We assume flat priors for the three biasing parameters, α_1 , α_2 , and σ_{b_s} , as well as for σ_{SN} . Each specific set of parameters together with one of the three mass distribution models generates a synthetic realization of the 50-source SNIa sample. From this entire ensemble of realizations, we only consider those that satisfy these observational constraints: (1) the total rms dispersion

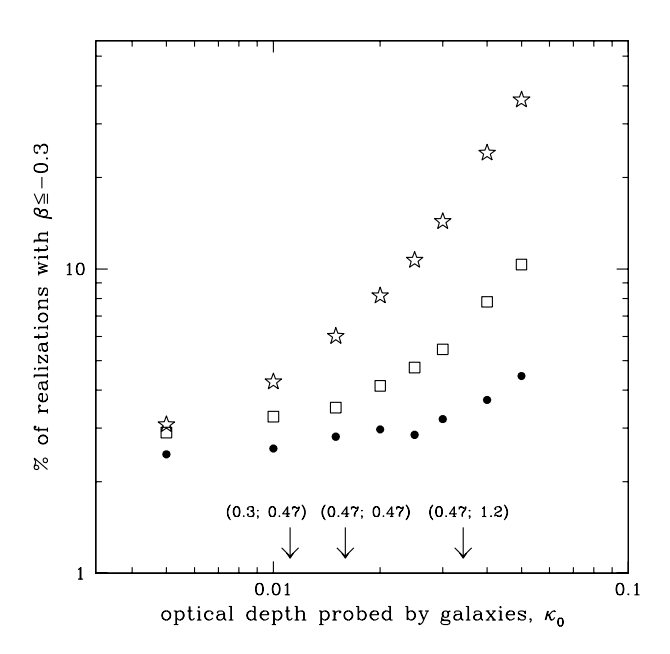


Figure 6. Probability of obtaining the observed results (slope β of the M_{SN} vs. $N_>/N$ relation) given different mass distribution models, and a range of optical depths. Solid dots assume standard κ pdf of Section 5.1.1, empty squares and star symbols represent bifocal I and II models, respectively, discussed in Section 5.1.2. Each point was obtained using 10,000 synthetic realizations of SNIa 50-source sample. See Section 6 for details.

in the synthetic SNIa magnitudes (which includes intrinsic and lensing induced contributions) must be within 0.05 mag of the actual observed value of 0.3mag; (2) the moments of the synthetic δn_{gal} distribution (average, standard deviation, skewness and kurtosis) must be reasonably close to those of the observed distribution, which is characterized by (0.063, 0.52, 1.7, 4.9). We chose "reasonably close" to mean that synthetic values must not be more than a factor of 2 away from the actual values. Because of these constraints, the range from which the values of α_1 , α_2 , σ_{b_s} , and σ_{SN} parameters are picked is not relevant, as long as it not too restrictive. In other words, the observational constraints eliminate cases with very large values of these parameters.

The data suggests that demagnified SNe are not lost due to the flux limit. If they were, we would have less SNe at small values of $N_>/N$, and more at high values of $N_>/N$, whereas in the data (Fig. 1) the sources are roughly equally spread over the entire $N_>/N$ range. So our synthetic lensing models assume that we do not lose SNe because of deamplification.

For each synthetic realization of the 50-source SNIa sample we derive the corresponding $M_{SN}-N_>/N$ relation. The slope of the best-fit line, β is recorded. For a given value of κ_0 we generate 10,000 realizations. Solid dots in Fig. 6 show the percentage of realizations that have β smaller than the observed value of -0.3, as a function of total optical depth, for the standard κ pdf. Empty squares and star symbols represent the results for the bifocal I and II.

Figure 6 considers a range of optical depths. What is the appropriate value for κ_0 ? If the source is at the median source redshift for our sample, $z_s = 0.47$, then APM galaxies

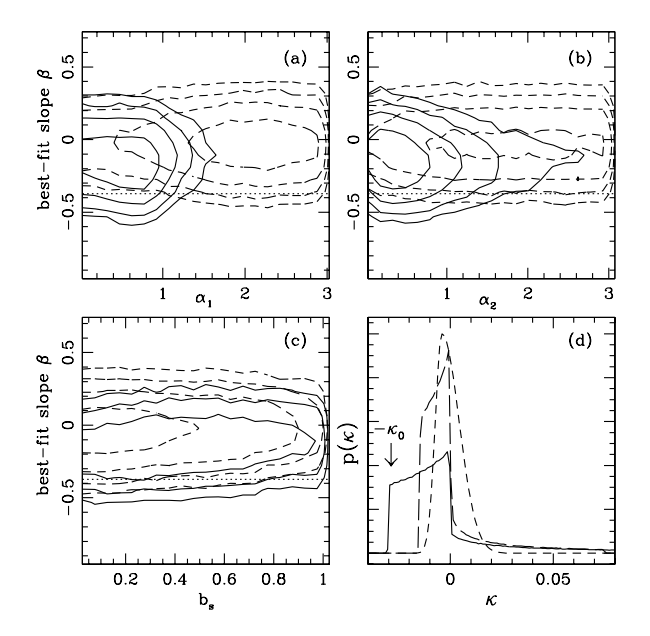


Figure 7. Panels (a)–(c) show the dependence of the best-fit slope of the M_{SN} – $N_{>}/N$ relation on the three biasing parameters (see Section 5.2). Short-dash lines are for the standard κ pdf model of Section 5.1.1, while the solid lines are for the bifocal II κ pdf described in Section 5.1.2. Both models assume optical depth $\kappa_0=0.03$. The contours are based on 50,000 realizations, and are spaced a factor of 3 apart. The shapes of the contours are partly determined by the observational constraints, described in Section 6 (second paragraph). It is evident that biasing parameters have little impact on the β . Panel (d): Short-dash and solid lines represent κ pdfs corresponding to the contours in panels (a)–(c) of the same line type. The minimum κ in the bifocal II pdf is $-\kappa_0$ (indicated by an arrow). The long-dash line represents bifocal I κ pdf.

sample the mass distribution up to a redshift of about 0.3. In this case the lensing optical depth probed by APM galaxies is 0.011 (left-most arrow in Fig. 6). A somewhat more optimistic estimate for κ_0 is obtained if we assume that galaxies trace the mass fluctuations up to the median source redshift, 0.47, which gives $\kappa_0 = 0.016$ (middle arrow). The limiting case is obtained by considering the most distant source, at $z_s = 1.2$, and assuming that galaxies probe mass up to a redshift of 0.47, which gives $\kappa_0 = 0.034$ (right-most arrow).

The important conclusion from this figure is that if the standard mass distribution (Section 5.1.1) is assumed, then the value of κ_0 does not really matter, and the probability of reproducing the observations is $\lesssim 3\%$, if κ_0 is within a reasonable range. If, on the other hand, the bifocal pdf I or II are assumed, the probability of reproducing observations depends sensitively on the assumed optical depth. If $\kappa_0 = 0.034$ then these models yield 6-20% probability. The bifocal pdfs produce more discernible lensing effects, for the same κ_0 because they have a wider range in A, as seen in Fig. 7(d).

The results presented in Fig. 6 marginalize over values of all the model parameters (except κ_0), so the effects of the biasing parameters on β are hidden. However, it turns out that these parameters do not correlate with β . Figure 7 shows the dependence of β on α_1 , α_2 and b_s for the bifocal II κ pdf model (solid contour lines), and the standard κ

pdf model (dashed contour lines), both for $\kappa_0 = 0.03$. Fifty thousand realizations were created for each model, and the corresponding contour lines plotted, with adjacent contours separated by a factor of 3. It is apparent that for both models the dependence on the biasing parameters is weak.

We conclude that the slope of the M_{SN} – $N_{>}/N$ relation depends on the amount and distribution of matter, i.e. on κ_0 and the shape of the κ pdf model, but does not depend on the specifics of the biasing scheme. Figure 6 quantifies the dependence on amount and distribution of mass: as expected, higher optical depth results in more pronounced lensing effects. Standard κ pdf produces less lensing for the same κ_0 compared to a much broader bifocal pdf. Figure 7 demonstrates that biasing has little effect on the slope of M_{SN} – $N_{>}/N$ relation. In other words, the type of lensing signature considered here $(M_{SN}-N_{>}/N$ relation for standard candles) probes mass distribution, and is independent of biasing.

7 CONCLUSIONS

We detect the signature of weak lensing in the current sample of 50 high redshift SNIa taken from two teams: High-z Supernova Search Team and Supernova Cosmology Project. After correcting SNe magnitudes for cosmological distances (assuming Tonry et al. (2003) values), we find that brighter SNe are preferentially found behind regions overdense in foreground galaxies. This $M_{SN}-N_{>}/N$ relation has a slope $\beta=-0.3$ to -0.4, when the angular radii of foreground regions are 5-15 arcmin. The statistical significance is >99% (see Fig. 4 and 5). The angular radii of 5-15 arcmin imply that the lensing structures are 1-3 $h_{0.7}^{-1}$ Mpc across if they are located at a redshift of 0.1, and so correspond to non-linearly evolved intermediate-scale structure.

Aside from the possibility that the observed M_{SN} $N_{>}/N$ relation is a fluke, there is one other possible, nonlensing interpretation: Galactic dust obscuration, which would make SNIa sources brighter and APM galaxies more numerous in the directions devoid of Galactic dust. If this interpretation is correct, then (1) Galactic extinction corrections applied to the SNe (Tonry et al. 2003) are much too small, and (2) Galactic dust is able to change projected APM galaxy number density by 50%, since the observed rms in δn_{gal} is ≈ 0.5 . We cannot comment on (1), but can estimate the effect of (2). How much excess/deficit in galaxy density can Galactic dust create? Using Schlegel et al. (1998) data we calculate the average A_B Galactic extinction for the 50 SNe sample to be 0.18 mag. The slope of the R-band APM galaxy number counts is $d \log N/dm = 0.35$, therefore typical "dust-induced" $(1+\delta n_{gal})=10^{A_B\cdot d\log N/dm}\approx 1.16$. This is an upper bound because extinction in the R band will be smaller than in A_B , and because extinction averaged over 5-15 arcmin radius patches will be smaller than estimates for individual SNe, given that Schlegel et al. (1998) extinction map resolution is 6'.1 FWHM. If Galactic dust is indeed the cause of the $M_{SN}-N_{>}/N$ correlation, then M_{SN} and $N_{>}/N$ should separately correlate with SNe extinction. In reality, Schlegel et al. (1998) extinction estimates do not show a correlation with either M_{SN} or $N_{>}/N$. Overall, Galactic dust interpretation of the observed $M_{SN}-N_{>}/N$ relation seems unlikely, but cannot be ruled out.

Note that dust *intrinsic* to the $z_l \sim 0.1$ structures

probed by the APM galaxies cannot be invoked to explain the observations, because such dust would produce an effect opposite to the one detected here, i.e. β would be positive. If dust is present in groups and clusters traced by the APM, it will diminish the amplitude of the effect we detect. Presence of dust in groups was suggested by Boyle et al. (1988) who found that faint QSO candidates are anti-correlated with foreground groups. However, such an anti-correlation can also be explained by weak lensing (Rodrigues-Williams & Hogan 1994; Croom & Shanks 1999). Current observations indicate that groups and clusters do not contain significant amounts of dust (Ferguson 1993; Nollenberg et al. 2003).

If the lensing interpretation in correct, then the standard models of mass distribution have some difficulty in reproducing β ; the observed value would be detected only in $\lesssim 3\%$ of the cases. We investigate how β is affected by the amount and distribution of mass along the light of sight to the sources, and galaxy biasing schemes.

We find that larger optical depths and broader κ pdf result in steeper β slopes (Fig. 6). Optical depth is a function of global geometry, and no realistic cosmological model can give $\kappa_0 \gtrsim 0.05$, which is what would be required to comfortably explain the results. Broader κ pdfs mean that mass fluctuations are more extreme than the standard cosmological models allow, a scenario which is in apparant conflict with other means of determining mass fluctuations, like cosmic velocity flows and weak shear lensing.

We also find that biasing has little effect on β (Fig. 7). This insensitivity to biasing is in contrast to weak lensing induced QSO-galaxy and GRB-galaxy (anti-)correlations, where biasing could, at least partly explain the higher than expected amplitude of the effect (Jain et al. 2003; Williams & Frey 2003). We conclude that weak lensing of standard candles provides a cleaner probe of the mass distribution at $z \lesssim 0.1$, on \sim few Mpc scales, then lensing induced angular correlations.

In fact, SNIa can provide the perfect means of measuring mass inhomogeneities using gravitational lensing. A set of standard candles at known redshifts can be analyzed using the complementary techniques of weak magnification and weak shear lensing. The advantage of magnification lensing over the more commonly used shear lensing is that with the former one can chose the redshift range of the lenses, whereas the latter yields the cumulative effect of lensing along the entire line of sight to the source. Therefore a large uniform set of intermediate redshift SNIa, such as the ones that would result from the SNAP mission³ and the LSST mission⁴ would be invaluable for the studies of mass clustering in the nearby Universe. In addition to detecting intermediate and high-redshift SNe for the purposes of estimating the global cosmological parameters and the equation of state of the dark energy, SNAP will also measure weak shear lensing signature due to large scale structure. Combining magnification data (of the type considered in this paper) and shear information (Rhodes et al. 2003) for a large set of SNe will allow the study of mass distribution at $z \lesssim 1.5$ with unprecedented accuracy and 3-dimensional spatial resolution.

The final issue we address is the impact of weak lensing on the determination of global cosmological parameters, Ω_m and Ω_Λ using SNIa standard candles. In principle, weak lensing can affect the derived values of Ω_m and Ω_{Λ} , if (1) demagnified SNe are preferentially lost from the sample due to faint flux cutoff, and/or (2) the κ pdf is asymmetric and the SN sample size is small (see also Wambsganss et al. (1997)). If demagnified SNe were lost from the sample then the distribution of SNe in $N_>/N$ would be skewed in the direction of larger N > /N values. If κ pdf is asymmetric, (and it is, on scales considered here), then most SNe in a small sample will be slightly demagnified compared to average, and will have their N > N skewed in the direction of smaller values. So both (1) and (2) would make the distribution of SNe in $N_>/N$ uneven, and would to some extent cancel each other. In the present sample of 50, the distribution of SNe in $N_>/N$ is indistinguishable from uniform, so the average M_{SN} corresponds to the average $N_>/N$, and hence lensing effects by ~Mpc-size structures probably did not bias the derived values of Ω_m and Ω_{Λ} .

ACKNOWLEDGEMENTS

The authors would like to thank Peter Garnavich and Jason Rhodes for their careful reading of the manuscript and valuable comments.

REFERENCES

Amanullah R., Mortsell E., Goobar A. 2003, A&A, 397, 819

Benitez N., Martinez-Gonzalez E. 1997, ApJ, 477, 27

Benitez N., Riess A., Nugent P., Dickinson M., Chornock R., Filippenko A. 2002, ApJ, 577, L1

Benitez N., Sanz J.L., Martinez-Gonzalez E. 2001, MN-RAS, 320, 241

Boyle, B. J., Fong, R. & Shanks, T. 1988, MNRAS, 231, 897

Cen R., Ostriker J.P. 1993, ApJ, 417, 415

Croom, S. M., & Shanks, T. 1999, MNRAS, 307, L17

Dekel A., Lahav O. 1999, ApJ, 520,24

Ferguson, H.C. 1993, MNRAS, 263, 343

Garnavich P.M. et al. 1998, ApJ, 493, L53

Holz D.E. 1998, ApJ, 506, L1

Holz D.E., Wald R.M. 1998, Phys. Rev. D, 58, 063501

Irwin M., Maddox S.J., McMahon R.G. 1994, Spectrum, 2, 14. See also http://www.ast.cam.ac.uk/~mike/apmcat/

Jain B., Scranton R., Sheth R.K. 2003,

preprint, http://xxx.lanl.gov/abs/astro-ph/0304203 Jain B., Seljak U., White S.D.M. 2000, ApJ, 530, 547

Kovner I. 1991, ApJ, 376, 70 Lewis G.F., Ibata R.A. 2001, MNRAS, 324, L25

Maddox S. J., Efstathiou G., Sutherland W.J. 1996, MN-RAS, 283, 1227

Metcalf R.B. 1999, MNRAS, 305, 746

Moertsell E., Gunnarsson C., Goobar A. 2001, ApJ, 561, 106

³ http://snap.lbl.gov

⁴ http://www.lsst.org/lsst_home.html

Nollenberg, J.G., Williams, L.L.R. & Maddox, S.J. 2003, AJ, 125, 2927

Refregier A. 2003, preprint,

http://lanl.arXiv.org/abs/astro-ph/0307212

Rhodes J., Refregier A., Massey R. & the SNAP Collaboration, priprint,

http://lanl.arXiv.org/abs/astro-ph/0304417

Rodrigues-Williams, L.L., & Hogan, C. 1994, AJ, 107, 451 Riess A. et al. 1998, AJ, 116, 1009

Schlegel D.J., Finkbeiner D.P., Davis M. 19998, ApJ, 500, 525

Tonry J. L. et al. 2003, preprint,

http://lanl.arXiv.org/abs/astro-ph/0305008

Perlmutter S. et al. 1999, ApJ, 517, 565

Wambsganss J., Cen R., Xu G., Ostriker J.P. 1997, ApJ, 475, L81

Williams L.L.R., Frey N. 2003, ApJ, 583, 594

Williams L.L.R., Irwin M. 1998, MNRAS, 298, 378